J. Fluid Mech. (1986), *vol.* 166, *pp.* 93–113
Printed in Great Britain

Model studies of the aortic pressure rise just after valve closure

By A. A. VAN STEENHOVEN AND M. E. H. VAN DONGEN
Departments of Mechanical Engineering and Physics, Eindhoven University of Technology, The Netherlands

(Received 12 July 1985 and in revised form 8 November 1985)

Model experiments are performed in a long, thin-walled, fluid-filled, latex tube in which the fluid is locally suddenly stopped, starting from a steady flow, thus simulating the wave phenomenon generated by the final closure of the aortic valve. The resulting waveform is determined as it propagates upstream. The effect of a local step-wise change in compliance close to the valve, representing the aortic sinus section, is investigated. The observed phenomena are analysed by means of a quasi-one-dimensional model, solved by the method of characteristics, taking into account the influence of nonlinearities, wall shear stress, viscoelastic wall properties and wave reflections. The theoretical computations are well confirmed by the experimental results. The pressure jump, induced by the valve closing, appeared to be slightly affected by nonlinearities. The decrease of the pressure jump while propagating upstream and the gradual pressure increase that follows the pressure jump are caused by the effect of wall shear stress. The local change in compliance generates the expected wave reflections and has a strong influence on the rise-time of the wave front. The experiments confirmed the prediction that wall viscoelasticity is the dominant factor in the gradual decay of the slope of the wave.

1. Introduction

The study of nonlinear wave propagation in liquid-filled viscoelastic tubes is often motivated by its application to arterial blood flow. It is known from both static and dynamic measurements (Bergel 1961; Milnor 1982) that the walls of the large blood vessels exhibit nonlinear elastic and viscous properties. The analysis of the resulting blood flow and pressure pulse waveforms at various locations in the arterial tree has been the subject of many investigations. Most often the approach has been mathematical. Important contributions have been given among others by Womersley (1957). For an overview of these studies we refer to Pedley (1980). More recently a detailed linear approach has been given by Kuiken (1984). The results of most of these mathematical models of arterial pulse propagation have been compared to in-vivo data, which is quite difficult in view of the many assumptions made in each model. Only a few data are available from well-defined model experiments. An outline of such experiments was given by Kivity & Collins (1974) in order to determine the viscoelastic properties of large blood vessels. Gerrard (1985) performed a series of measurements of the longitudinal wall motion in water-filled latex tubes, induced by an oscillating flow, in order to verify Womersley's predictions and to investigate the influence of local tethering at the tube end.

In the present paper the wave phenomena in a long latex tube are described and analysed following a jump in pressure. The physiological relevance of this study apart

from gaining more insight into wave propagation in the arterial system, is more specifically the understanding of the phenomena that occur just after aortic valve closure. Bellhouse & Talbot (1969), van Steenhoven & van Dongen (1979) and van Steenhoven *et al.* (1982), among others, analysed the closing behaviour of this valve in more detail. When the natural valvular closing mechanism is disturbed, for example when a bioprosthesis is used, the necessary back flow to complete the closure increases considerably. The reversed flow early in diastole may then increase from 2 % to 25 % of the total forward flow ejected during systole. This back flow is suddenly slowed down by the closing aortic valve, which causes a rise in the aortic pressure known as the dicrotic notch. Sauren *et al.* (1983) demonstrated that the valve leaflets are much stiffer than the aortic wall. The latter in turn differs slightly in elasticity from the sinus walls. Moreover, all these tissues show remarkable visco-elastic material properties. It is the ultimate goal of this study to determine the parameters which govern the pressure rise just after valve closure, with reference both to its magnitude and slope close to the valve and its propagation through the aorta. As a first step, in the present model study sudden valve closure is simulated, starting from a steady initial flow, and the resulting pressure rise is studied in relation to the wall material properties, the initial volume flow rate, the distance to the valve and a negative or positive reflection coefficient at a distinct point (like the sinus–aorta connection) in the tube. First the experimental set-up and some qualitative experimental observations are presented. Next some physical models based on one-dimensional wave propagation in flexible tubes are considered. Finally, a quantitative comparison of theoretical predictions with experimental data is given.

2. Qualitative experimental observations

2.2. *The experimental set-up*

The basic set-up consists of a latex tube (Penrose Drain, length ≈ 0.6 m, internal diameter ≈ 18 mm, wall thickness ≈ 0.2 mm) fixed between two reservoirs, see figure 1 (*a*). The tube is slightly pre-stressed in the axial direction and supported by a rigid flat plane. The fluid used is water. Collapse of the tube is prevented by a transmural pressure p_0 of 3 kPa adjusted by the fluid height in the reservoirs. At $x = 0$ the diameter of the latex tube is locally 20 % reduced by means of a Perspex ring. From the left reservoir a metal tube (outer diameter = 8 mm) is aligned along the axis of the latex tube, the tip of it being located at the constriction at $x = 0$. From this tip towards the right reservoir four nylon threads (diameter = 50 μm) are stretched. Over these threads a rigid washerlike occluder (outer diameter = 16 mm, internal diameter = 6.5 mm, specific weight = 10^3 kg/m^3) can be taken along by the flow. A rapid reduction of the volume flow to zero is achieved at the moment that the occluder contacts both the constriction of the latex tube and the tip of the previously mentioned metal tube (closing time ≈ 15 ms).

The experimental procedure was as follows. First a transmural pressure of about 3 kPa was applied, causing a radial pre-strain of about 7 %. Starting from this situation the steady-state relation between area and pressure was determined. Next, a constant fluid flow was established from the right to the left reservoir with a velocity between 0.1 and 0.5 m/s. The corresponding Reynolds number had a value between 1800 and 9000 so that in most cases the flow was turbulent. The wave experiment was started by releasing the occluder, at the upstream end of the set-up, so that it is taken along by the flow. At the moment the occluder contacts the constriction,

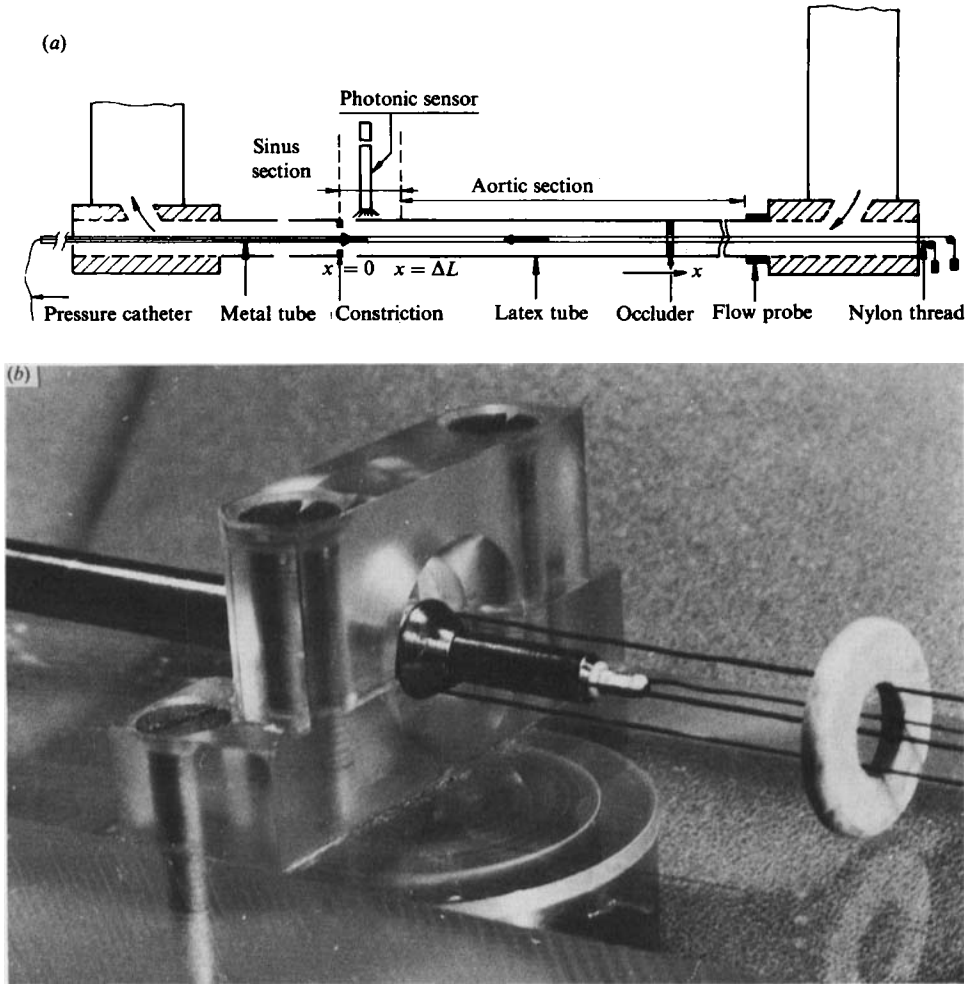

FIGURE 1. The experimental set-up: (*a*) schematical drawing and (*b*) photograph of the constriction point when the latex tube is removed.

the flow is stopped, causing a jump in pressure and cross-sectional area which propagates upstream. The time- and position-dependence of pressure were measured locally on the axis of the tube with a catheter-tip manometer (Millar PC 470) which was positioned through the metal tube as shown in figure 1(*b*). The catheter cross-section is 3% of that of the tube. Its influence on the wave phenomena is neglected. To determine the wavefront distortion two catheter-tip manometers were used simultaneously, one close to the constriction and the other, analogously inserted at the right-hand side, at a distance of a multiple of 50 mm from the former. To measure the wall deflection during the pressure jump a photonic sensor (MTI KD-100) was used, placed about 1 mm above the tube itself. The value of volume flow was measured electromagnetically (Transflow 601) at the inflow end of the tube. All electrical signals were recorded on an electromagnetic tape recorder (Hewlett–Packard 3968 A) and the pressure and wall deflection signals were analysed using a two-channel transient recorder (Datalog 912). From the simultaneous measurement of the time dependent pressure and tube diameter, the visco-elastic properties of the tube were

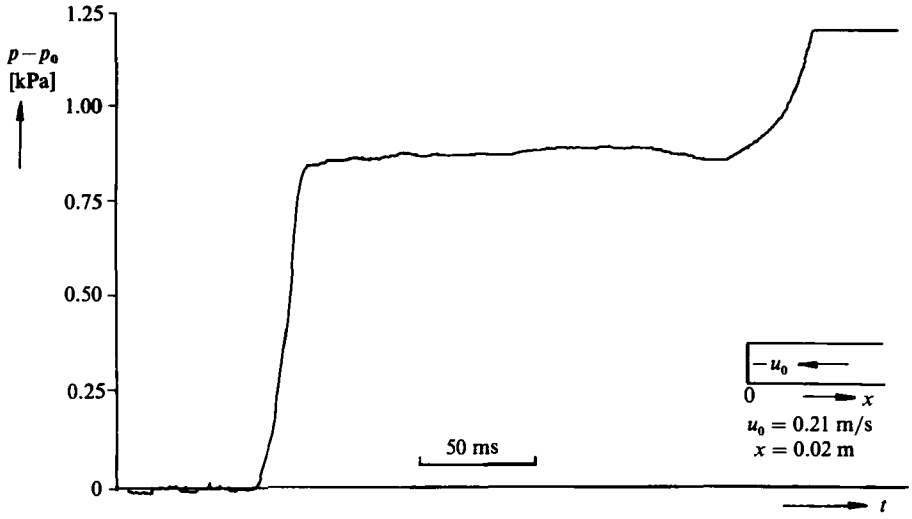

FIGURE 2. Typical tracing of the pressure jump measured close to the valve ($p_0 = 3$ kPa).

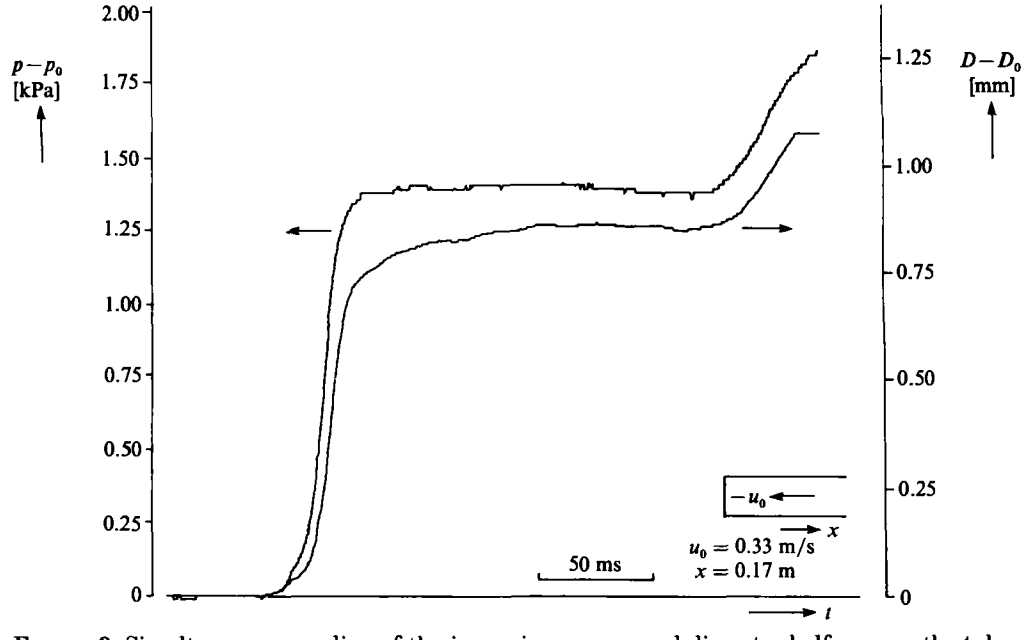

FIGURE 3. Simultaneous recording of the jumps in pressure and diameter half-way up the tube ($p_0 = 3$ kPa, $D_0 = 17.12$ mm).

deduced, see §4. Direct measurements of the tube wall properties by cyclic uniaxial tensile experiments confirmed the presence of viscous effects, but no reliable data pertaining to the strain rates (2 s^{-1}) and frequencies (0–40 Hz) of interest were obtained. The wave experiments were performed at various values of initial fluid velocity and initial pressure. Also the presence of a sinus region close to the valve was simulated. By telescoping one latex tube into another a local change in wall thickness of a factor 2 was achieved. Two situations were realized: a compliant thin-walled sinus section of 0.04 m length adjacent to the valve connected to a less compliant aorta and vice versa.

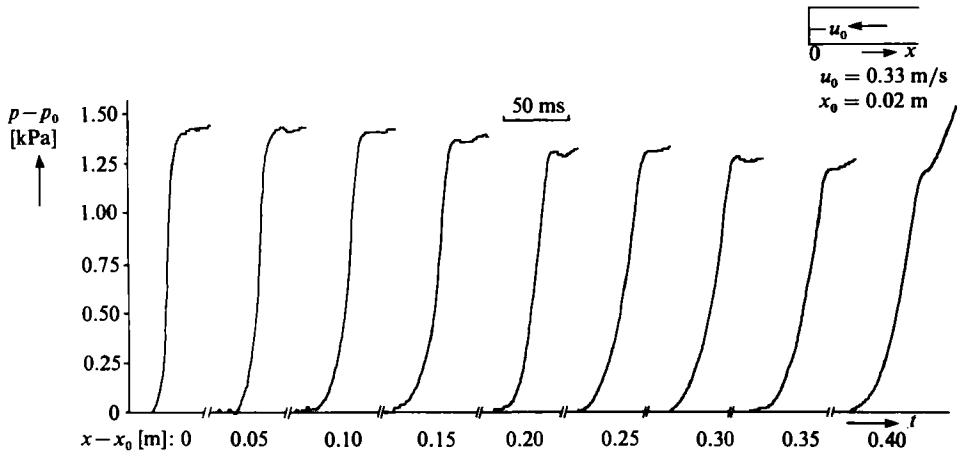

FIGURE 4. The pressure waveform as a function of position ($p_0 = 3$ kPa).

2.2. *Characteristic results*

A typical result of the pressure signal in a uniform tube and close to the valve is given in figure 2. As a result of valve closure the pressure rapidly increases. The rise time of the wavefront is about 15 ms and is caused by the finite closing time of the occluder. This initial fast pressure jump is followed by a much more gradual increase, after which the pressure signal shows a second rapid increase caused by the wave reflection at the upstream reservoir. In figure 3 a simultaneous recording of the jumps in pressure and diameter 0.17 m upstream of the valve is given. This illustrates the close relationship between area and pressure changes and is used to determine the pressure–area relationship of the tube during the jump. In figure 4 the pressure waveform is shown at different positions. From these waveforms it is seen that the rise-time of the wavefront increases with distance from the occluder. Furthermore, the pressure jump appears to decrease slightly while propagating upstream. Finally, some characteristic wave-reflection results are given in figure 5. The right-hand tracing of figure 5 (*a*) gives the pressure jump close to the valve for the case in which the 'sinus' is more compliant than the 'aorta'. As a reference the left half gives the pressure jump in a uniform tube. Due to the compliant 'sinus' region the rise time of the pressure close to the valve is found to be increased. Similarly, figure 5 (*b*) gives the pressure jump for the case in which the 'sinus' is less compliant than the 'aorta'. Then pressure oscillations close to the valve are observed. In the next section some physical models will be presented to interpret these experimental observations.

3. Physical models

3.1. *Basic equations*

The observed wave phenomena can be described mathematically by the one-dimensional laws of mass and momentum for a straight uniform flexible tube, see Lighthill (1978) and Pedley (1980):

$$\frac{\partial}{\partial x}(uA)+\frac{\partial A}{\partial t}=0, \quad \frac{\partial u}{\partial t}+u\frac{\partial u}{\partial x}+\frac{1}{\rho}\frac{\partial p}{\partial x}=\frac{2\tau}{\rho R}. \tag{1a,b}$$

Here u, p denote the cross-sectional average of axial velocity and pressure; x is the axial coordinate; t is time; η and ρ are viscosity and density of the fluid; $\tau = \eta(\partial u/\partial r)|_R$

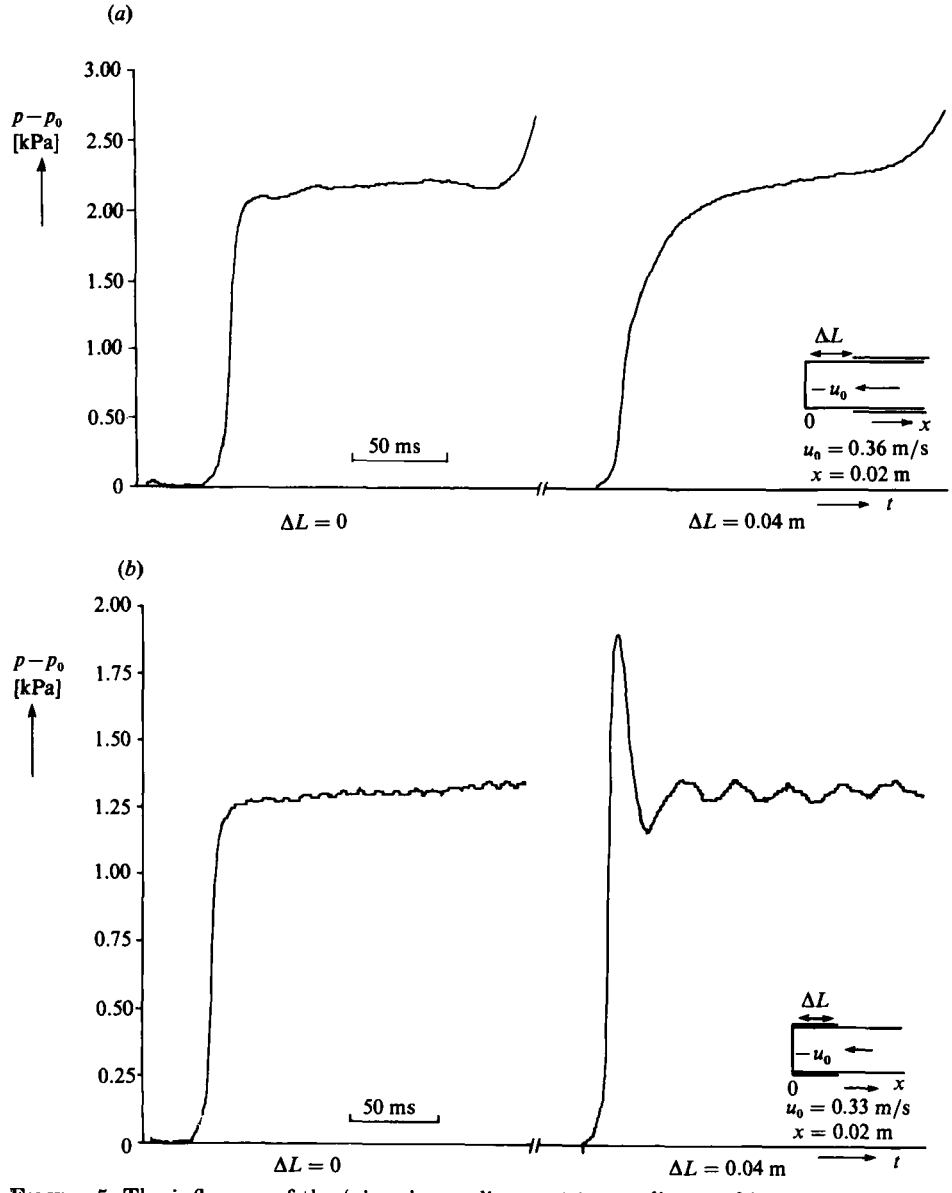

FIGURE 5. The influence of the 'sinus' compliance: (*a*) compliance of 'sinus' is increased and (*b*) compliance of 'sinus' is decreased, both with respect to the reference situation on the left ($p_0 = 3$ kPa).

is the wall shear stress and $A = \pi R^2$ is the cross-sectional area. The assumption of one-dimensionality leading to equation (1) holds if the wavelengths of all disturbances of interest are long compared to the diameter. In our case the main wavelength associated with the axial extent of the wavefront is estimated to be about six times the tube diameter. Besides, the difference between the cross-sectional average of the axial velocity squared and the square of the average axial velocity is neglected, which is a reasonable approximation for the turbulent flow situation at hand. The radial pressure variation is also neglected which is certainly valid far from the wavefront. Within the front a small radial variation of the pressure of the order of 5 % is possible.

We will assume here that the phenomena observed are well described by the set of equations (1).

In order to describe the wall behaviour we follow Kivity & Collins (1974) by introducing the following tube law:

$$p = f(A) + g(A)\frac{\partial A}{\partial t}. \tag{2}$$

Now we define the compliance per unit length c, the wave speed a and a new variable ν:

$$c^{-1} = \frac{\partial f}{\partial A}, \quad a^2 = \frac{A}{\rho c}, \quad \nu = \int_{A_{00}}^{A} \frac{a}{A}\,\mathrm{d}A, \tag{3}$$

where A_{00} is the initial cross-sectional area at $x = 0$. In a steady state or if visco-elasticity is neglected, i.e. $g(A) = 0$, the definition of ν can also be written as

$$\nu = \int_{p_{00}}^{p} \frac{1}{\rho a}\,\mathrm{d}p, \tag{4}$$

where p_{00} is the initial pressure at the valve. Inserting these definitions in (1), and after some rearrangement we obtain the following characteristic set:

$$\left(\frac{\partial}{\partial t} + (u \pm a)\frac{\partial}{\partial x}\right)(u \pm \nu) = -\frac{1}{\rho}\left(\frac{\partial g}{\partial A}\frac{\partial A}{\partial t}\frac{\partial A}{\partial x} + g\frac{\partial^2 A}{\partial x\,\partial t}\right) + \frac{T}{\rho}. \tag{5}$$

The + signs refer to the right-running characteristics (c^+), while the − signs refer to the left-running characteristics (c^-). T, which equals $2\tau/R$, will be specified later on. Besides, one of the equations (5) can also be used in combination with the continuity equation to give

$$\frac{\partial \nu}{\partial t} + u\frac{\partial \nu}{\partial x} + a\frac{\partial u}{\partial x} = 0. \tag{6}$$

This set of equations needs to be completed with the initial and boundary conditions:

$$u = -u_0, \quad \nu = \nu_0 = \frac{T_0 x}{\rho a_0} \quad (t \leqslant 0), \tag{7a}$$

$$u = u_v(t) \quad (x = 0, t \geqslant 0). \tag{7b}$$

The subscript 0 will represent the initial state. The velocity $u_v(t)$ represents the time-dependent fluid velocity at $x = 0$ imposed by the closing valve. The small initial variation in ν means a small variation in initial cross-sectional area A_0. Its influence on initial velocity is neglected.

We shall now discuss the nonlinear inviscid solution, some aspects of wall shear stress, the influence of wall viscoelasticity and reflections due to tube inhomogeneities. For the sake of simplicity and clarity each of these effects will be treated separately. The treatment of nonlinear effects is described, e.g. by Pedley (1980), while the effects of wall shear stress and wall viscoelasticity are treated on the basis of wave coordinates according to Whitham (1974).

3.2. *Nonlinear inviscid case*

Neglecting shear stresses and wall viscosity, (5) read

$$\left(\frac{\partial}{\partial t} + (u \pm a)\frac{\partial}{\partial x}\right)(u \pm \nu) = 0. \tag{8}$$

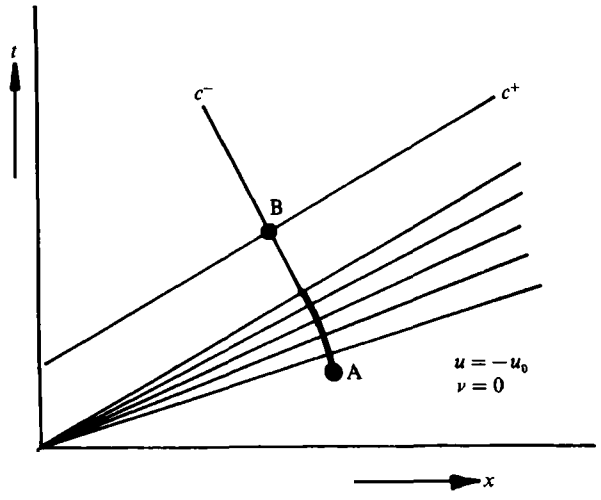

FIGURE 6. $x-t$ diagram in the case of nonlinear elastic tube behaviour.

The initial condition is then $u = -u_0$, $\nu = 0$ for $t \leqslant 0$ and the boundary condition at $x = 0$ is $u = 0$ for $t \geqslant 0$, so $u_v(t)$ is assumed here to be a step function. Applying the invariance of $u-\nu$ to the arbitrary points A and B in the uniform regions separated by the wavefront (see figure 6), we obtain

$$\nu_B = u_0. \tag{9}$$

We can approximate ν, defined by (4), with $p_{00} = p_0$, by assuming a linear relation between a and p:

$$a = a_0(1-\alpha(p-p_0)), \tag{10}$$

with $|\alpha(p-p_0)| \ll 1$. Then

$$\nu = \frac{1}{\rho a_0}\{(p-p_0)+\tfrac{1}{2}\alpha(p-p_0)^2\}, \tag{11}$$

and the solution for the jump in pressure becomes

$$\Delta p = p_B - p_0 = \rho a_0 u_0(1-\tfrac{1}{2}\alpha\rho a_0 u_0). \tag{12}$$

For the latex tube $\alpha > 0$, so the jump becomes smaller due to the nonlinearity.

The distortion of the wavefront, expressed in terms of the increase in rise-time, follows from the difference in $(u+a)$ between the top and the foot of the wave. To first order we find, using (10) and (12),

$$\Delta t = \frac{\Delta(u+a)}{a_0^2}x = \left(\alpha\rho - \frac{1}{a_0^2}\right)u_0 x. \tag{13}$$

As was already pointed out by Olsen & Shapiro (1967), the wave travels undistorted if $\alpha\rho a_0^2 = 1$, which is approximately valid for latex.

Finally we consider the influence of initial pressure p_0 on wavefront velocity, by raising p_0 with regard to a reference pressure p_{ref}. Again we assume $|\alpha(p_0-p_{ref})| \ll 1$ and

$$a_0 = a_{ref}(1-\alpha(p_0-p_{ref})). \tag{14}$$

To first order in pressure we then find for the velocity of the wavefront centre

$$\left(\frac{\Delta x}{\Delta t}\right)_c = a_{ref}\left\{1-\frac{1}{2}\frac{u_0}{a_{ref}}-\alpha(\tfrac{1}{2}\rho a_{ref}u_0+(p_0-p_{ref}))\right\}. \tag{15}$$

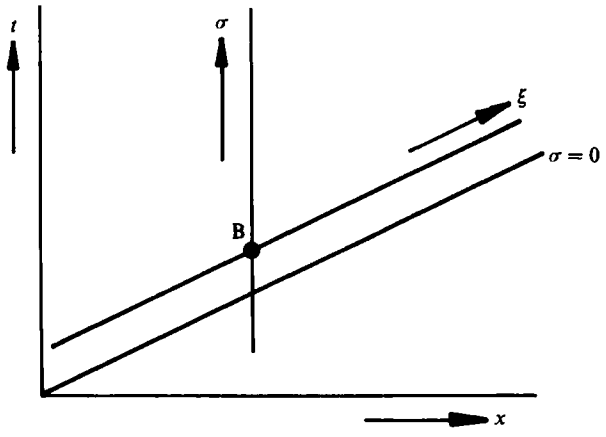

FIGURE 7. Introduction of the wave-coordinates ξ and σ.

3.3. *Some aspects of wall shear stress and viscoelasticity*

In their linearized form, the set of equations (5) can be written as

$$\left(\frac{\partial}{\partial t}\pm a_0\frac{\partial}{\partial x}\right)(u-v)=\frac{T}{\rho}+\frac{A_0 g_0}{\rho}\frac{\partial^2 u}{\partial x^2}=S, \tag{16}$$

where the source term S, which is assumed to be small, represents the right-hand side. In order to analyse the problem we introduce the following reduced variables (see figure 7):

$$\epsilon=\frac{S_0 t_0}{u_0},\quad \xi=\epsilon\frac{x}{a_0 t_0},\quad \sigma=\frac{a_0 t-x}{a_0 t_0},\quad \hat{u}=\frac{u}{u_0},\quad \hat{v}=\frac{v}{u_0},\quad \hat{S}=\frac{S}{S_0}, \tag{17}$$

where t_0 is a characteristic time for the jump and S_0 some typical value of S. The time coordinate σ is the time elapsed since the passage of the wavefront, ξ is chosen such that the variations along the wave are of order unity. Introducing the new variables in (16) for the right-running characteristic and in the linearized equation (6) yields

$$\frac{\partial}{\partial\xi}(\hat{u}+\hat{v})=\hat{S}, \tag{18}$$

$$\frac{\partial\hat{v}}{\partial\sigma}-\frac{\partial\hat{u}}{\partial\sigma}=-\epsilon\frac{\partial\hat{u}}{\partial\xi}. \tag{19}$$

The initial and boundary conditions, denoting the initial value of the source term by $\hat{S}_i$, become

$$\hat{u}=-1,\quad \hat{v}=\hat{S}_i\xi \quad \text{for } \sigma\to-\infty, \tag{20a}$$

$$\hat{u}=\hat{u}_v(\sigma) \qquad \text{for } \xi=0. \tag{20b}$$

Now $\hat{v}$, $\hat{u}$ and $\hat{S}$ are expanded in the small parameter ϵ:

$$\hat{u}=\hat{u}^{(0)}+\epsilon\hat{u}^{(1)}+\ldots,\quad \hat{v}=\hat{v}^{(0)}+\epsilon\hat{v}^{(1)}+\ldots,\quad \hat{S}=\hat{S}^{(0)}+\epsilon\hat{S}^{(1)}+\ldots.$$

Inserting this in (18) and (19) and equating terms of equal power in ϵ yields

$$\frac{\partial}{\partial\sigma}(\hat{v}^{(0)}-\hat{u}^{(0)})=0,\quad \frac{\partial}{\partial\xi}(\hat{v}^{(0)}+\hat{u}^{(0)})=\hat{S}^{(0)}, \tag{21a,b}$$

$$\frac{\partial}{\partial\sigma}(\hat{v}^{(1)}-\hat{u}^{(1)})=-\frac{\partial\hat{u}^{(0)}}{\partial\xi},\quad \frac{\partial}{\partial\xi}(\hat{v}^{(1)}+\hat{u}^{(1)})=\hat{S}^{(1)}. \tag{22a,b}$$

It is easily found from (21) and (20a) that

$$\hat{v}^{(0)} = \hat{u}^{(0)} + 1 + \xi \hat{S}_1, \quad \frac{\partial \hat{u}^{(0)}}{\partial \xi} = \tfrac{1}{2}(\hat{S}^{(0)} - \hat{S}_1). \tag{23a,b}$$

At the valve, where $\hat{u}^{(1)} = 0$, it follows from (22a) and (23a) that

$$\hat{v}^{(1)} = -\frac{1}{2}\int_{-\infty}^{\sigma} (\hat{S}^{(0)} - \hat{S}_1)\, \mathrm{d}\sigma' \quad (\xi = 0). \tag{24}$$

Equation (23b) will be used to describe the development of the waveform while propagating upstream. Equations (23a) and (24) describe the pressure signal close to the valve.

3.3.1. *Wall shear stress*

Let us first assume that the source consists of wall shear stress only and that there is no viscoelasticity. In that case $\hat{v}$ is directly related to pressure, $\hat{v} = (p - p_{00})/(\rho a_0 u_0)$. We will take the initial shear force T_0 as a reference: $S_0 = T_0/\rho$, and $\hat{S}_1 = 1$. In general $\hat{T} = T/T_0$ can be written as the sum of a steady part $\hat{T}_s$, which depends on velocity only, and an unsteady part, $\hat{T}_u$. For the unsteady shear stress we will take the flat boundary-layer solution for a time-dependent semi-infinite flow. This leads to the following approximation for $\hat{T}_u$:

$$\hat{T}_u = -\frac{2}{\pi^{\frac{1}{2}}} \frac{\rho u_0}{T_0} \left(\frac{\eta}{\rho R^2 t_0}\right)^{\frac{1}{2}} \int_0^{\sigma} \frac{\partial \hat{u}}{\partial \sigma}(\sigma') \frac{1}{(\sigma - \sigma')^{\frac{1}{2}}}\, \mathrm{d}\sigma'. \tag{25}$$

This approximation is expected to be valid if the unsteady viscous penetration depth $(\eta \sigma t_0/\rho)^{\frac{1}{2}}$ is much smaller than the velocity gradient length of the initial flow $(2\eta u_0/T_0 R)$, or stated otherwise if $\hat{T}_u \gg 1$, even if the initial flow is turbulent. For laminar tube flow, the relative error of approximation in (25) is, according to Zielke (1968), of the order of 4.4 $(\eta \sigma t_0/\rho R^2)^{\frac{1}{2}}$.

Since the acceleration is large only within the wavefront, where the velocity changes from a value -1 to a value $\hat{u}^-(\xi)$ say, we shall represent $\partial \hat{u}/\partial \sigma$ by

$$\frac{\partial \hat{u}}{\partial \sigma} = \begin{cases} \hat{u}^- + 1 & (0 \leqslant \sigma \leqslant 1), \\ 0 & (\sigma < 0, \sigma > 1). \end{cases} \tag{26}$$

Then, the expression for the source term becomes

$$\hat{S} = \hat{T}_s - \frac{4}{\pi^{\frac{1}{2}}} \frac{\rho u_0}{T_0} \left(\frac{\eta}{\rho R^2 t_0}\right)^{\frac{1}{2}} (\hat{u}^- + 1) \begin{cases} \sigma^{\frac{1}{2}} & (0 \leqslant \sigma \leqslant 1), \\ \{\sigma^{\frac{1}{2}} - (\sigma - 1)^{\frac{1}{2}}\} & (\sigma > 1). \end{cases} \tag{27}$$

It will be shown in the next section, that the unsteady part of $\hat{S}$ is indeed dominant within the wavefront. By inserting (27) into (23b) for $\sigma = 1$, and neglecting the steady part of $\hat{S}$, we obtain the following equation for the velocity at $\sigma = 1$:

$$\frac{\partial \hat{u}^-}{\partial \xi} = -\frac{2}{\pi^{\frac{1}{2}}} \frac{\rho u_0}{T_0} \left(\frac{\eta}{\rho R^2 t_0}\right)^{\frac{1}{2}} (1 + \hat{u}^-). \tag{28}$$

A similar result holds for v, and thus for the pressure, so that we may write in dimensional variables

$$\Delta p = p^- - p_0 = \rho a_0 u_0 \exp\left(-\frac{x}{L}\right), \quad L = \tfrac{1}{2} a_0 \left(\frac{\rho \pi R^2 t_0}{\eta}\right)^{\frac{1}{2}}. \tag{29a,b}$$

By combining (27), (23*a*) and (24) and using $\hat{u}_v = 0$, $\hat{T}_s(0) = 0$, we find for the pressure at the valve after closure:

$$\frac{p-p_{00}}{\rho a_0 u_0} = 1+\frac{4}{3}\left(\frac{\eta t_0}{\rho\pi R^2}\right)^{\frac{1}{2}}\left\{\left(\frac{t}{t_0}\right)^{\frac{3}{2}}-\left(\frac{t}{t_0}-1\right)^{\frac{3}{2}}\right\}+\frac{1}{2}\frac{T_0 t}{\rho u_0} \quad (x=0,\, t\geqslant t_0). \tag{30}$$

Hence, as a result of wall shear stress the pressure jump will decay exponentially while propagating upstream and the pressure at the valve will gradually increase after the initial jump.

3.3.2. *Wall viscoelasticity*

If only viscoelasticity is important an appropriate choice for the reference value S_0 is

$$S_0 = \frac{A_0 g_0 u_0}{(\rho a_0^2 t_0^2)}, \quad \text{while } \hat{S}_i = 0. \tag{31}$$

The source term $\hat{S}$, rewritten in wave coordinates, is in zeroth order in ϵ

$$\hat{S}^{(0)} = \frac{\partial^2 \hat{u}^{(0)}}{\partial\sigma^2}. \tag{32}$$

In this case (23*b*) is a simple diffusion equation for $\hat{u}^{(0)}$. Since $\hat{v}^{(0)} = 1+\hat{u}^{(0)}$ the same holds for $\hat{v}^{(0)}$:

$$\frac{\partial\hat{v}^{(0)}}{\partial\xi} = \frac{1}{2}\frac{\partial^2\hat{v}^{(0)}}{\partial\sigma^2}. \tag{33}$$

A suitable solution representing a jump-like behaviour of $\hat{v}^{(0)}$ is

$$\hat{v}^{(0)} = -\tfrac{1}{2}\operatorname{erfc}\frac{\sigma}{2^{\frac{1}{2}}(\xi+\xi_0)^{\frac{1}{2}}}+1. \tag{34}$$

The parameter ξ_0 accounts for the finite rise-time of the jump at $\xi = 0$. In order to investigate the decay of the slope of the wavefront, we define the rise-time as follows:

$$\Delta\sigma = \left(\frac{\partial\hat{v}^{(0)}}{\partial\sigma}\right)^{-1}_{\sigma=0}; \quad \Delta\sigma_0 = \left(\frac{\partial\hat{v}^{(0)}}{\partial\sigma}\right)^{-1}_{\sigma=0,\,\xi=0}. \tag{35}$$

It is easily found from (34) that, in dimensional form,

$$\frac{\Delta t}{\Delta t_0} = \frac{\Delta\sigma}{\Delta\sigma_0} = \left(1+\frac{2\pi g_0 A_0}{\rho a_0^3(\Delta t_0)^2}x\right)^{\frac{1}{2}}. \tag{36}$$

Finally, by inspection of (23*a*), (24) and (32) it is found that viscoelasticity does not contribute to v after valve closure, and consequently it does not modify the pressure jump at the valve.

A separate treatment of nonlinear effects, wall viscoelasticity and shear force is only possible if the effects are not strong and do not interfere. For the present situation this is a rather good assumption. The only significant effect of nonlinearity is a somewhat reduced value of the pressure jump at the valve; shear stress and viscoelasticity have no such effect. Viscoelasticity causes a diffusion-like broadening of the wavefront, the two other factors have no significant influence. Wall shear stress induces a decay of the pressure jump when the wavefront propagates upstream. Here there is some interference. The characteristic decay length contains the rise-time of the jump which increases by viscoelasticity.

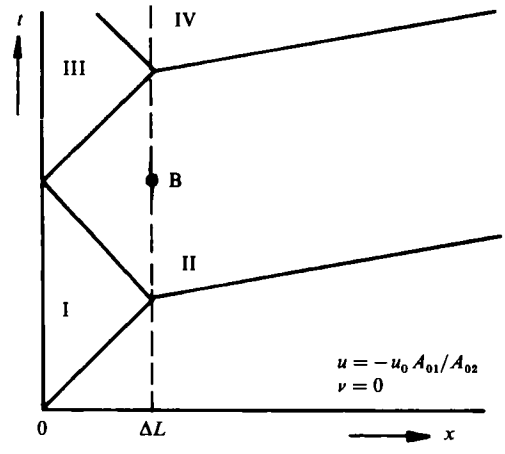

FIGURE 8. $x-t$ diagram in the case of a tube inhomogeneity.

3.4. *Wave reflections*

Suppose two regions of different wall properties and cross-sectional areas and assume that the change of properties occurs in a distance l satisfying the compactness condition $l/a_{0i}t_0 \ll 1$, $i = 1, 2$. The inviscid, elastic and linearized equations (5) read

$$\left(\frac{\partial}{\partial t} \pm a_{0i}\frac{\partial}{\partial x}\right)\left(u_i \pm \frac{p_i}{\rho a_{0i}}\right) = 0 \quad (i = 1, 2), \tag{37}$$

with $a_{0i} = (A_{0i}/\rho c_{0i})$. The initial and boundary conditions (7) reduce to:

$$u_1 = -u_0, \quad u_2 = -u_0 A_{01}/A_{02}, \quad p_i = p_0 \quad (t \leqslant 0), \tag{38a}$$

$$u_1 = 0 \qquad (x = 0, t \geqslant 0). \tag{38b}$$

Continuity of pressure and flow at the interface ($x = \Delta L$) implies:

$$p_1(\Delta L, t) = p_2(\Delta L, t), \quad u_1(\Delta L, t)\, A_{01} = u_2(\Delta L, t)\, A_{02}. \tag{39a, b}$$

We further introduce as reflection coefficient:

$$R = \frac{Z_2 - Z_1}{Z_2 + Z_1} \quad \text{with } Z_i = \frac{\rho a_{0i}}{A_{0i}}. \tag{40}$$

Let x_1, x_2 be arbitrary positions in regions 1 and 2 respectively and define the time intervals Δt_1 to Δt_4 as:

$$\Delta t_1 = \frac{x_1}{a_{01}}, \quad \Delta t_2 = 2\,\frac{(\Delta L - x_1)}{a_{01}}, \quad \Delta t_3 = \frac{\Delta L}{a_{01}} + \frac{x_2 - \Delta L}{a_{02}}, \quad \Delta t_4 = \frac{2\Delta L}{a_{01}}. \tag{41}$$

Combination of a c^+-characteristic in region 1 and a c^--characteristic in region 2 (see figure 8) using (39) then leads directly to the pressure solution in the two regions as function of time:

t	p_1	t	p_2
$0 \to \Delta t_1$	p_0	$0 \to \Delta t_3$	p_0
$\to \Delta t_1 + \Delta t_2$	$p_0 + \rho a_{01} u_0$	$\to \Delta t_3 + \Delta t_4$	$p_0 + (1+R)\rho a_{01} u_0$
$\to 3\Delta t_1 + \Delta t_2$	$p_0 + (1+R)\rho a_{01} u_0$	$\to \Delta t_3 + 2\Delta t_4$	$p_0 + (1+2R+R^2)\rho a_{01} u_0$.
$\to 3\Delta t_1 + 2\Delta t_2$	$p_0 + (1+2R)\rho a_{01} u_0$		
$\to 5\Delta t_1 + 2\Delta t_2$	$p_0 + (1+2R+R^2)\rho a_{01} u_0$		
$\to 5\Delta t_1 + 3\Delta t_2$	$p_0 + (1+2R+2R^2)\rho a_{01} u_0$		

(42)

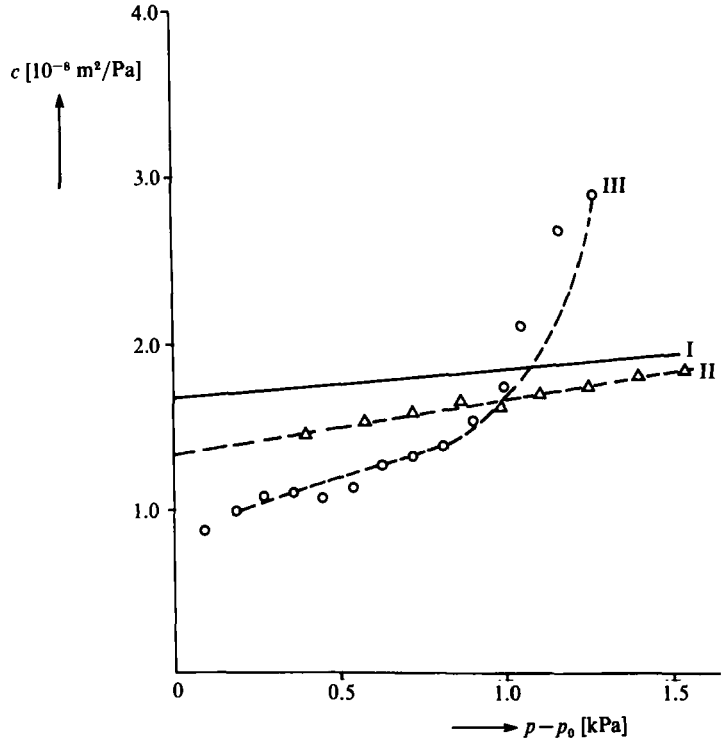

FIGURE 9. Tube compliance versus pressure: I static and II dynamic values. III corresponds to the time dependent values during the pressure jump ($p_0 = 3$ kPa, $A_0 = 2.30\ 10^{-4}$ m^2). The dotted lines correspond to the best-fit.

The limiting value in both regions equals $p_0 + \rho a_{0_2} u_0 A_{0_1}/A_{0_2}$. Hence a positive reflection coefficient ($Z_1 < Z_2$) causes a gradual increase of the pressure in both regions, while for a negative value of R ($Z_1 > Z_2$) the pressure will vary in an oscillatory manner.

4. Verification of theory

4.1. *Determination of wall properties*

To verify the theory, the material constants α, defined by (10), and the viscoelastic parameter g_0 have to be determined. To that end, first a steady state relation between A and p was determined and the corresponding compliance $c_1 = \mathrm{d}A/\mathrm{d}p$ is depicted in figure 9 versus the pressure difference $p - p_0$. The second procedure was to determine the incremental values of ΔA and Δp over the wave jump, defined as the increases with regard to the initial state at about 100 ms after the jump front, from wave experiments with $u_0 = 0.2$ m/s. We will refer to $c_2 = \Delta A/\Delta p$ as the dynamic compliance. By raising the initial pressure, the pressure dependence of c_2 shown in figure 9 was determined. The observed difference between the dynamic and static compliances is an indication of the presence of small low-frequency viscoelastic effects. Similar behaviour is known to occur in arteries (Bergel 1961*a*, *b*). The wave speeds, $a = (A/\rho c)^{\frac{1}{2}}$, corresponding to the static (I) and dynamic (II) values of the compliances are well represented by: I $a = 3.71$ m s^{-1}, II $a = 4.11\{1 - 0.53\ 10^{-4}(p - p_0)\}$ m s^{-1}. Hence, according to (10), $a_0 = 3.71$ m s^{-1}, $\alpha = 0$ for the first and $a_0 = 4.11$ m s^{-1},

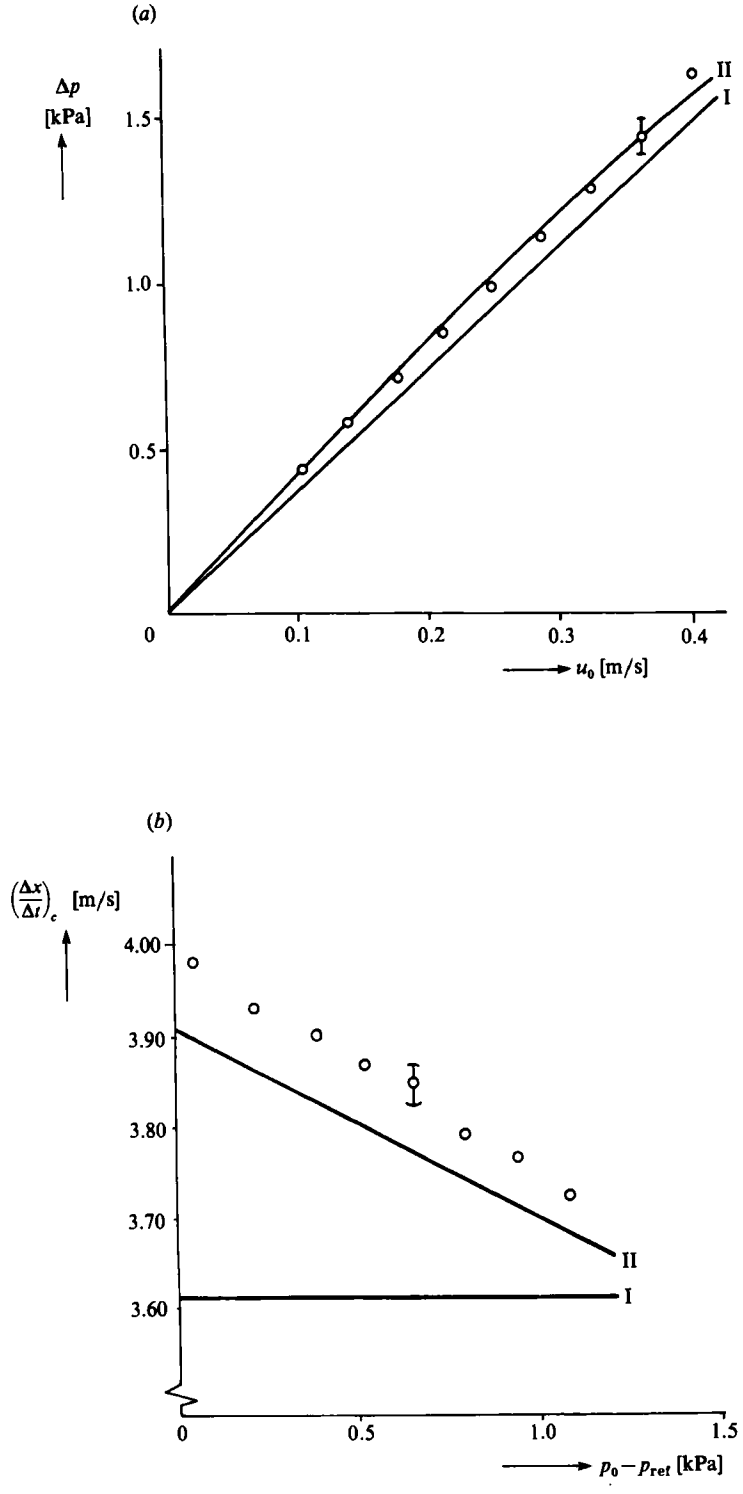

FIGURE 10(a,b). For caption see facing page.

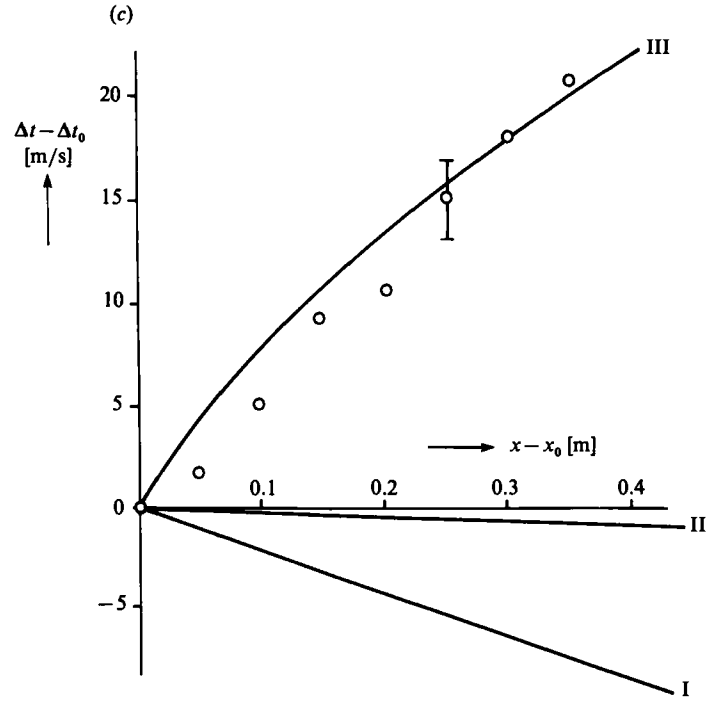

FIGURE 10. Influence of nonlinearities and wall viscoelasticity: (*a*) the pressure jump as function of the initial velocity ($x = 0.02$ m), (*b*) the velocity of the wavefront centre as function of the initial pressure ($u_0 = 0.21$ m s^{-1}, $p_{\text{ref}} = 3$ kPa), (*c*) the rise-time of the wavefront as function of position ($u_0 = 0.33$ m s^{-1}, $\Delta t_0 = 13$ ms, $x_0 = 0.02$ m). The solid lines correspond to the theoretical prediction: I, II nonlinear theory (equations (12), (15) and (13)) based on static and dynamic compliances, respectively and III viscoelastic theory (equation (36)).

$\alpha = 0.53\ 10^{-4}$ Pa^{-1} for the second case. Thirdly, in order to calculate g_0, the time-dependent values of diameter and pressure of one experiment were used to calculate $c_3 = A'/p'$, where a prime denotes differentiation with respect to time. Inserting this definition into the linearized version of the viscoelastic model equation (see (2)), this results in

$$c_3 = \frac{c}{(1+g_0 cA''/A')}. \tag{43}$$

Of course c_3 is not a material property, but depends on time through A''/A'. For the recordings of figure 3 this means that for the low-pressure part of the wavefront $A'' > 0$, and c_3 will be less than c; for the high-pressure part of the front $A'' < 0$ and c_3 will exceed c. This effect is indeed demonstrated in figure 9, where c_3 for the experiment of figure 3 has been plotted as a function of $p(t) - p_0$. In (43), the dynamic value c_2 is inserted, since this is considered to be some average value in the frequency range of interest. By means of a best-fit procedure, a value for g_0 was obtained of $1.3\ 10^5$ N s m^{-4}. The corresponding best-fit for c_3 as a function of $p(t) - p_0$ is also shown in figure 9.

Cowley (1982) reports that for the determination of the tube law a distinction has to be made between the tethered and untethered situation. In the latter case an explicit time dependence can enter the tube law even for a purely elastic wall material. In the present experiment, no significant longitudinal wall motion was observed, so

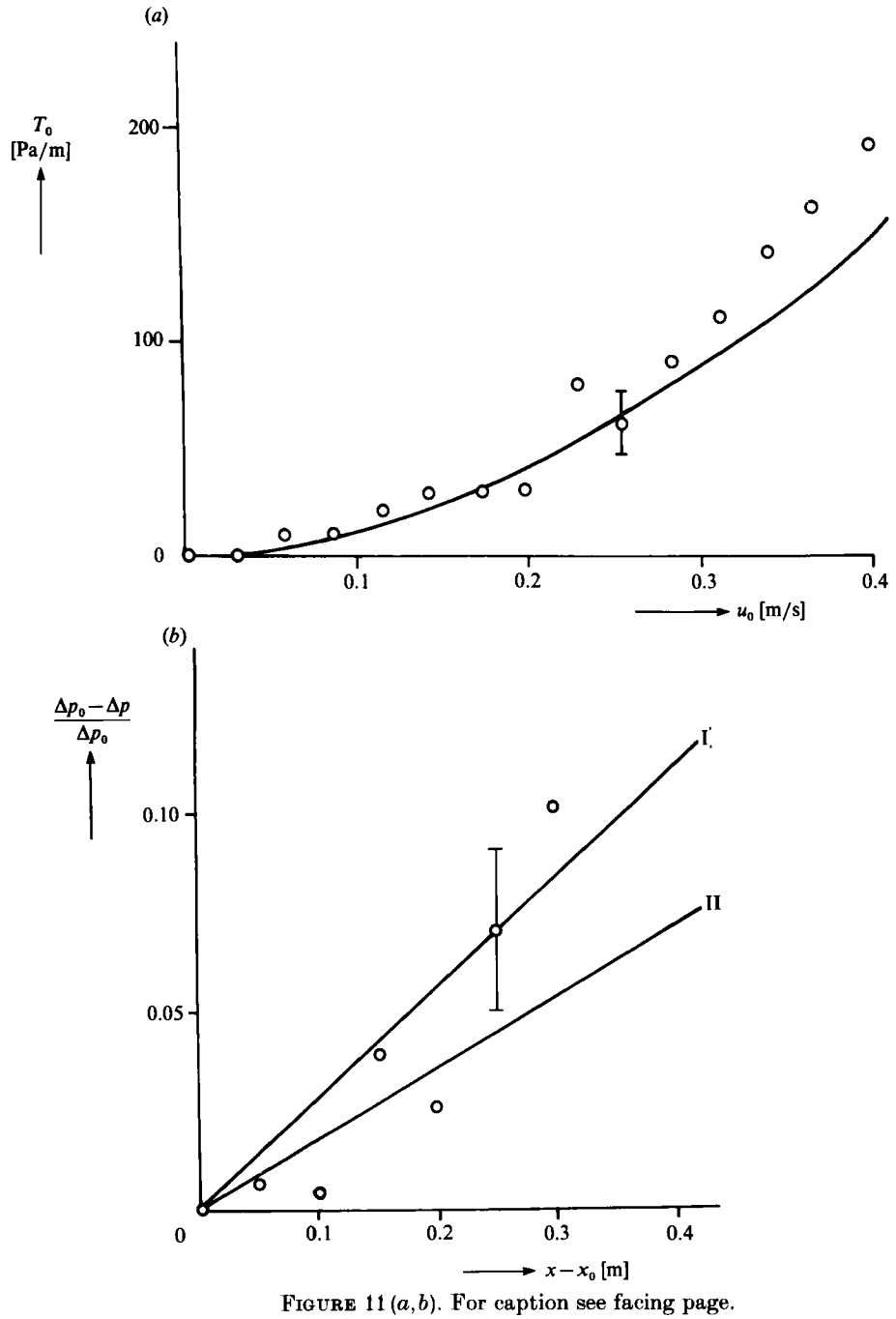

FIGURE 11 (*a*, *b*). For caption see facing page.

that the time dependence of the tube law is attributed to the viscoelastic properties of the latex material. It is interesting to compare the obtained value of g_0 with the values of the ratio of imaginary and real part of the Young's modulus E_i and E_r at different angular frequencies ω as reported by Gerrard (1985). From the definition of g in (2) and the inverse proportionality between compliance and Young's modulus, it follows that approximately the following relation holds: $E_i/E_r \approx cg_0\omega \approx 2\ 10^{-3}\omega$.

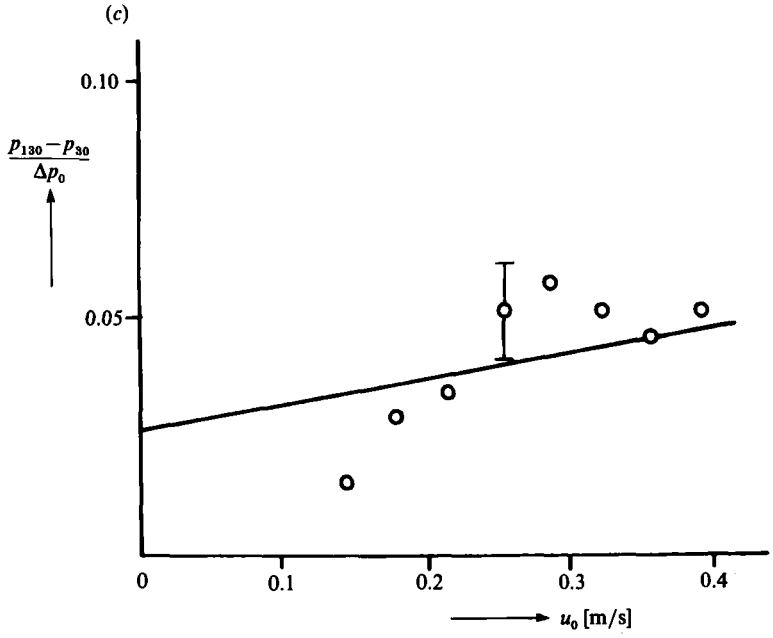

FIGURE 11. Influence of wall shear stress: (*a*) the initial wall shear stress as a function of the initial velocity determined from the pressure drop over a uniform tube of 0.8 m length; (*b*) the decay of the pressure jump as a function of position ($u_0 = 0.33$ m s^{-1}, $\Delta p_0 = 1.45$ kPa, $x_0 = 0.02$ m); (*c*) the reduced pressure increase close to the valve between 30 and 130 ms after valve closure as a function of the initial velocity ($x = 0.02$ m). The solid lines correspond to the theoretical prediction (equations (44), (29) and (30)): I, II in (*b*) are based on $t_0 = 13$ and 30 ms, while in (*c*) $t_0 = 13$ ms was used.

There is a remarkable agreement between this result and that of Gerrard up to frequencies of 4 Hz, although g_0 was obtained in a completely different manner at a much higher characteristic frequency.

4.2. *Influence of nonlinearities and wall viscoelasticity*

According to (12), (13) and (15) the nonlinearities affect the pressure jump, the rise-time of the wavefront at position x and the velocity of the wavefront centre, while wall viscoelasticity affects the rise-time of the wavefront according to (36). The pressure jump close to the valve, defined as the pressure increase within about 30 ms after valve closure, was measured as a function of the initial velocity, the result of which is given in figure 10(*a*). The inaccuracy of measurement is also indicated, based on a 95% reliability interval. The agreement between theory and experiment is close, especially when the dynamic values of the compliance are used. The dependence of the velocity of the wavefront centre on the initial velocity is difficult to measure due to the restricted range of adjustable initial velocities. Hence the initial state was changed by raising the initial pressure. The result of this experiment is shown in figure 10(*b*), together with the prediction according to (15). Here again the agreement is fair. Finally, the rise-time of the wavefront, defined by the time interval between 5 and 95% of the value of the jump, is determined as a function of position from waveforms like those shown in figure 4. Nonlinear theory based on the values of both static and dynamic compliances predicts that the waveform with initial rise-time Δt_0 would travel almost undistorted, which is in contrast with the experimental results,

see figure 10(*c*). By substitution of the value of g_0 given above into (36), we obtain a theoretical prediction of the decay of the slope of the wave due to the effect of wall viscoelasticity. In this way a local observation of the relation between A and p yields a prediction of the change in waveform as a function of position. The rise-time thus obtained is also plotted in figure 10(*c*), showing that viscoelasticity is indeed the dominant factor. The agreement between theory and experiment is quite satisfactory, considering the crudeness of the viscoelastic model applied.

4.3. *Influence of wall shear stress*

The main influences of the wall shear stress as predicted from theory are the gradual decay of the pressure jump as a function of position (equation (29)) and the steady increase of the pressure after the jump front (equation (30)). For the theoretical prediction a value of the initial wall shear stress is necessary. This value was estimated from the turbulent-flow pressure-loss relation (Schlichting 1979):

$$T_0 = \lambda \frac{1}{4} \frac{\rho u_0^2}{R} \quad \text{with } \lambda = 0.316\, Re^{-0.25}. \tag{44}$$

A verification of this relation at the Reynolds numbers occurring in our set-up, was performed by the pressure-drop measurement over a uniform tube of 80 cm length, the result of which is given in figure 11(*a*). If we substitute that in (27), we find, for a value of $t = t_0 = 13$ ms and $u_0 = 0.3$ m/s, that the ratio of T_u and T_0 is 7, which means that within and immediately behind the wavefront the assumption leading to (28) is justified.

The decay of the pressure jump as a function of position, predicted by theory, is observed in the experiments as shown in figure 11(*b*), where Δp_0 is the initial value of the pressure jump at $x = 0$. Due to viscoelastic effects the rise-time of the pressure jump increases from 13 ms close to the valve to 30 ms at $x = 0.3$ m (see figure 10*c*). Hence in figure 11(*b*) two theoretical predictions are given based on these two values of t_0. Agreement between theory and experiment is quite satisfactory. Next, the gradual pressure increase after the jump was measured close to the valve as a function of the initial velocity. The reduced pressure increase between 30 and 130 ms after valve closure, defined as $(p_{130} - p_{30})/\Delta p_0$, is plotted in figure 11(*c*) as a function of the initial velocity. The unsteady wall shear stress gives a contribution which is, according to (30), independent of initial velocity. The contribution of the initial wall shear stress (equation (44)) is approximately proportional to velocity, and is found to be smaller than the unsteady term. The total effect is quite small, of the order of a few per cent. The agreement between theory and experiment is fair.

4.4. *Influence of 'sinus' compliance*

Finally, the observed wave reflections in figure 5 can be explained from linear theory through (42). The reflection coefficient R was calculated from (40) under the assumption that the wave speed in both sections is proportional to the square root of the ratio of wall thickness and tube diameter. In figure 12(*a*) the jump is shown in the compliant 'sinus' case. At the left the pressure jump is shown in the 'sinus' and at the right the one in the 'aorta'. Due to the small length of the 'sinus' region in comparison with the wavelength a monotonic increase of pressure is found, which however converges quite well to the theory line. In case of a stiffer 'sinus' region, see figure 12(*b*), both theory and experiment show large oscillations close to the valve and smaller ones in the 'aorta'.

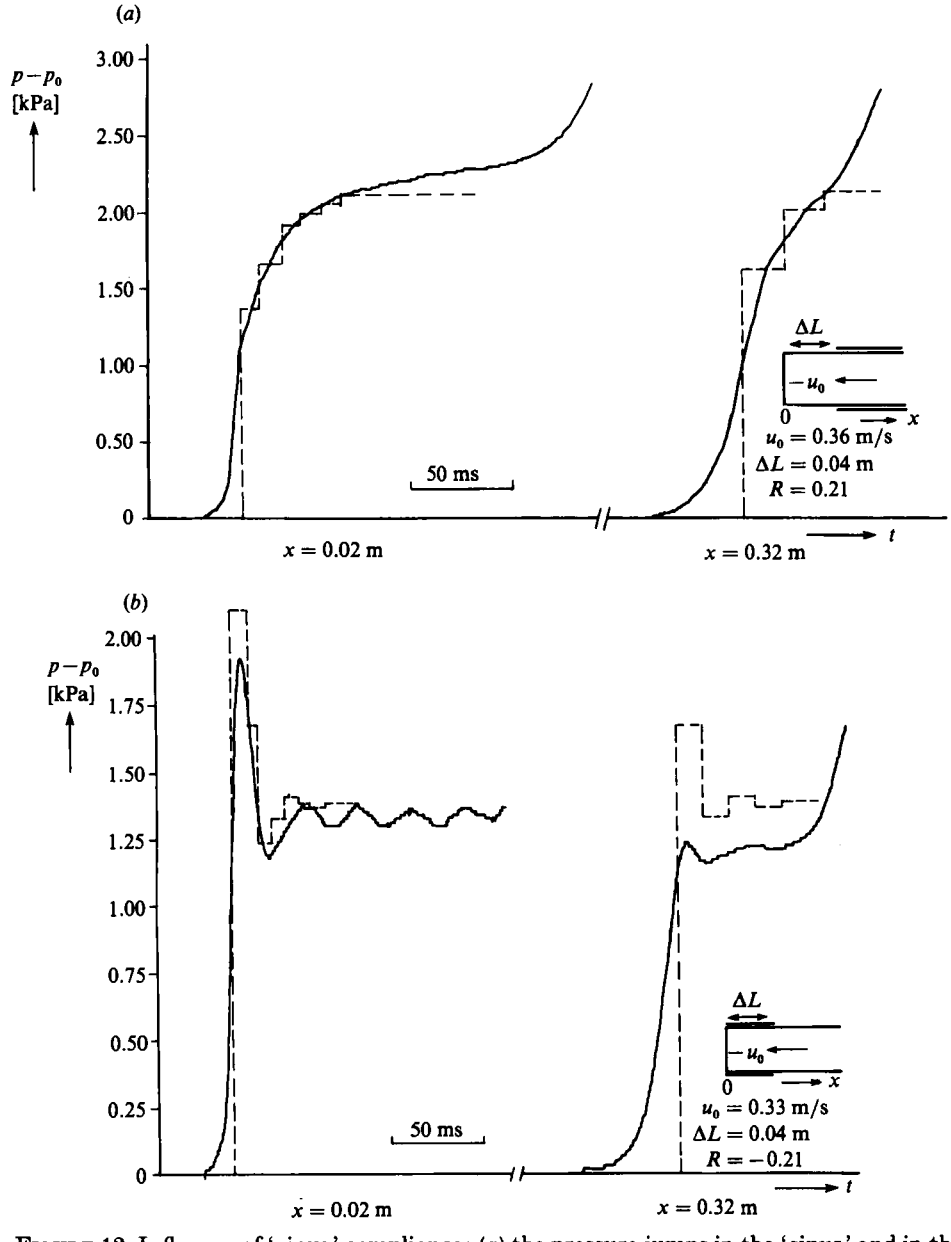

FIGURE 12. Influence of 'sinus' compliance: (*a*) the pressure jumps in the 'sinus' and in the 'aorta' when the compliance of the 'sinus' is increased and (*b*) when the compliance of the 'sinus' is decreased with respect to that of the 'aorta'. The dotted lines correspond to the theoretical prediction (equation (42)).

5. Concluding discussion

The present model experiments show that wave phenomena in a long uniform tube can be determined accurately by means of the present experimental method and that they are well described by the one-dimensional laws of mass and momentum. The pressure increase, induced by the valve closing, is slightly affected by nonlinearities. In the inhomogeneous case the compliance of the 'sinus' region strongly affects the

rise-time of the wavefront. The experiments also indicate that wall viscoelasticity is the dominant factor in the gradual flattening of the waveform. The rapid deceleration of the fluid element within the wavefront causes a locally large value of wall shear stress. The most important consequence is that the pressure jump of the wavefront decays while propagating upstream. At the valve the pressure keeps slightly increasing after the initial jump.

To interpret the experimental observations an analytical approach was followed based on the method of characteristics. The effects of nonlinearities, wall shear stress and wall viscoelasticity could be treated separately, since for the present situation these effects are not strong and do not interfere. There is only some interference between wall shear stress and wall viscoelasticity with regard to the decay of the pressure jump when the wavefront propagates upstream.

The difference that was observed between the dynamic and static compliances is an indication of the presence of small low-frequency viscoelastic effects. Obviously, the dynamic compliance, being some average value in the frequency range of interest, appeared to be the most relevant for the present experiments. The simple viscoelastic model used, appears to give a satisfactory description of the behaviour of the latex material during the jump. Of course the low-frequency, large-time behaviour cannot be described by such a simple model. In that case a more sophisticated constitutive description of the wall material, e.g. that of Holenstein, Nerem & Niederer (1984), should be applied. Such a model could also explain the transition from 'static' to 'dynamic' compliance.

With regard to the medical implications of this study it is stated that the magnitude of the pressure rise just after valve closure is primarily determined by the backflow velocity. Hence it is worth developing a prosthetic leaflet valve which exhibits the natural, gradual way of closure. Furthermore, the magnitude as well as the rise-time of the pressure jump close to the valve is strongly determined by the differences in compliance between the sinus region and the aortic one. Therefore, it is important that in the case of a prosthetic leaflet valve the sinus region remains compliant and that it is not stiffened due to the operation procedure.

We wish to thank Professor dr. ir. J. D. Janssen and Professor dr. ir. G. Vossers for their valuable comments and Mr J. W. G. Cauwenberg, Ing. Th. J. A. G. van Duppen and Ing. L. H. G. Wouters for their technical and laboratory assistance. We also thank all those students who contributed to this project.

REFERENCES

BELLHOUSE, B. J. & TALBOT, L. 1969 The fluid mechanics of the aortic valve. *J. Fluid Mech.* **35**, 721–735.

BERGEL, D. H. 1961*a* The static elastic properties of the arterial wall. *J. Physiol.* **156**, 445–457.

BERGEL, D. H. 1961*b* The dynamic elastic properties of the arterial wall. *J. Physiol.* **156**, 458–469.

COWLEY, S. J. 1982 Elastic jumps on fluid-filled elastic tubes. *J. Fluid Mech.* **116**, 459–473.

GERRARD, J. J. 1985 An experimental test of the theory of waves in fluid-filled deformable tubes. *J. Fluid Mech.* **156**, 321–347.

HOLENSTEIN, R., NEREM, R. M. & NIEDERER, P. 1984 On the propagation of a wavefront in viscoelastic arteries. *J. Biomech. Engng* **106**, 115–122.

KIVITY, Y. & COLLINS, R. 1974 Steady state fluid flow in viscoelastic tubes. Application to blood flow in human arteries. *Arch. Mech.* **26**, 921–931.

KUIKEN, G. D. C. 1984 Wave propagation in a thin-walled liquid-filled initially stressed tube. *J. Fluid Mech.* **141**, 289–308.

LIGHTHILL, M. J. 1978 *Waves in Fluids*. Cambridge University Press.

MILNOR, W. R. 1982 *Hemodynamics*. Williams and Wilkins.

OLSEN, J. H. & SHAPIRO, A. H. 1967 Large-amplitude unsteady flow in liquid-filled elastic tubes. *J. Fluid Mech.* **29**, 513–538.

PEDLEY, T. J. 1980 *The Fluid Mechanics of Large Blood Vessels*. Cambridge University Press.

SAUREN, A. A. H. J., VAN HOUT, M. C., VAN STEENHOVEN, A. A., VELDPAUS, F. E. & JANSSEN, J. D. 1983 The mechanical properties of porcine aortic valve tissues. *J. Biomech.* **16**, 327–337.

SCHLICHTING, H. 1979 *Boundary Layer Theory*. McGraw-Hill.

VAN STEENHOVEN, A. A. & VAN DONGEN, M. E. H. 1979 Model studies of the closing behaviour of the aortic valve. *J. Fluid Mech.* **90**, 21–36.

VAN STEENHOVEN, A. A., VAN DUPPEN, TH. J. A. G., CAUWENBERG, J. W. G. & VAN RENTERGHEM, R. J. 1982 In vitro closing behaviour of Björk-Shiley, St-Jude and Hancock heart valve prostheses in relation to the in-vivo recorded aortic valve closure. *J. Biomech.* **15**, 841–848.

WHITHAM, G. B. 1974 *Linear and Nonlinear Waves*. Wiley-Interscience.

WOMERSLEY, J. R. 1957 An elastic tube theory of pulse transmission and oscillatory flow in mammalian arteries. *Tech. Rep.* WADC-TR-56-614.

ZIELKE, W. 1968 Frequency-dependent friction in transient pipe flow. *J. Basic Engng* **90**, 109–115.